J. metamorphic Geol., 2005, **23,** 65–74 doi:10.1111/j.1525-1314.2005.00562.x

Formation of elliptical garnet in a metapelitic enclave by melt-assisted dissolution and reprecipitation

A. M. ÁLVAREZ-VALERO,[1] B. CESARE[1,2] AND L. M. KRIEGSMAN[3]
[1]*Department of Mineralogy and Petrology, University of Padova, Corso Garibaldi 37, I-35137 Padova, Italy (antonio.alvarezvalero@unipd.it)*
[2]*CNR - IGG Istituto di Geoscienze e Georisorse, Corso Garibaldi 37, I-35137 Padova, Italy*
[3]*National Museum of Natural History/Naturalis, PO Box 9517, NL-2300 RA Leiden, The Netherlands*

ABSTRACT Metapelitic residual enclaves in the Neogene Volcanic Province of SE Spain are residues left after melt extraction. Glass (quenched melt) of granitic composition occurs as inclusions in most minerals and as intergranular pockets. The most common enclave types show one stage of garnet growth that is interpreted to have occurred at the same time as glass production. Some of these show a well-developed foliation outlined by fibrolite, biotite, graphite and glass, which wraps around elongate garnet crystals that have aspect ratios up to 10:1. Based on microstructures and chemistry, the garnet within these rocks shows clear core and mantle structure. The core has an average composition of Alm_{76}–Prp_{08}–Sps_{14}–Grs_{03} and contains primary inclusions of biotite and melt, trapped during garnet growth. A thin (*c.* 100 μm), irregular mantle overgrows the garnet core, enclosing oriented fibrolite inclusions in strain caps, and biotite in strain shadows. In places, the overgrowths form skeletal elongated arms, which extend parallel to the foliation. The garnet mantle contains less Mn and higher X_{Mg}, but both core and mantle display flat Mn profiles, the contact being a sharp break. Ternary feldspar and Grt–Bt thermometry yield temperatures in the range 800–900 °C, with no systematic differences among the different microstructural domains of elliptical garnet. Based on the observed intracrystalline microstructures, the high amount of melt extraction in the rock by flattening component strain and the chemical zoning of garnet, the formation of elliptical garnet is modelled by a multistage sequence. This involves pressure solution and reprecipitation of the core, followed by post-kinematic, partly mimetic growth of the garnet mantle.

Key words: anatexis; El Hoyazo; elliptical garnet; enclave; pressure solution.

INTRODUCTION

Garnet is a mineral that generally forms equidimensional crystals, although elongate garnet has locally been observed in high-grade migmatites and granulites, as well as under diagenetic conditions. Their formation has been attributed to various mechanisms: (i) crystal ductile deformation (Ji & Martignole, 1994; Kleinschrodt & Mcgrew, 2000); (ii) oriented syntectonic growth (Kamb, 1959), or mimetic growth restricted to a pre-existing foliation; (iii) pressure solution (Passchier & Trouw, 1996; Den Brok, 1998), especially during diagenesis (Sprunt & Nur, 1977; Tada & Siever, 1989; Twiss & Moores, 1992; Ji & Martignole, 1996; Passchier & Trouw, 1996).

The first mechanism can be inferred by using orientation contrast (OC) images in a scanning electron microscope (SEM) (Prior *et al.*, 1999), which upon displaying weakly misoriented subgrains within the garnet, would be indicative of crystal plasticity. Oriented growth can be shown by textural relationships with inclusion minerals, in relation to internal and external foliations (Kamb, 1959).

Evidence for pressure solution is the presence of truncated features, such as primary inclusion patterns or chemical zoning patterns (Passchier & Trouw, 1996). Pressure solution and solution transfer processes have been widely described (e.g. Sprunt & Nur, 1977; Tada & Siever, 1989; Twiss & Moores, 1992; Ji & Martignole, 1996; Passchier & Trouw, 1996) as dominant events at diagenetic to low-grade metamorphic conditions (e.g. greenschist facies) where fluids are abundant and intragranular deformation mechanisms are relatively difficult. Little or no information exists on pressure-solution phenomena at high-grade conditions, especially in partially melted systems.

This work demonstrates that in the enclaves of El Hoyazo lava, in southern Spain, elliptical garnet has formed by a glass-present multiple process. This involves simultaneous pressure solution and (re)precipitation of the core, followed by post-kinematic, partly mimetic growth of the garnet mantle. These growth steps are related to the magma residence and eruption history of the El Hoyazo volcano.

GEOLOGICAL SETTING

The Neogene Volcanic Province (NVP) of southern Spain is situated in the Internal Zones of the Alborán Domain in the western Mediterranean (Fig. 1), and is a product of the complex geodynamic

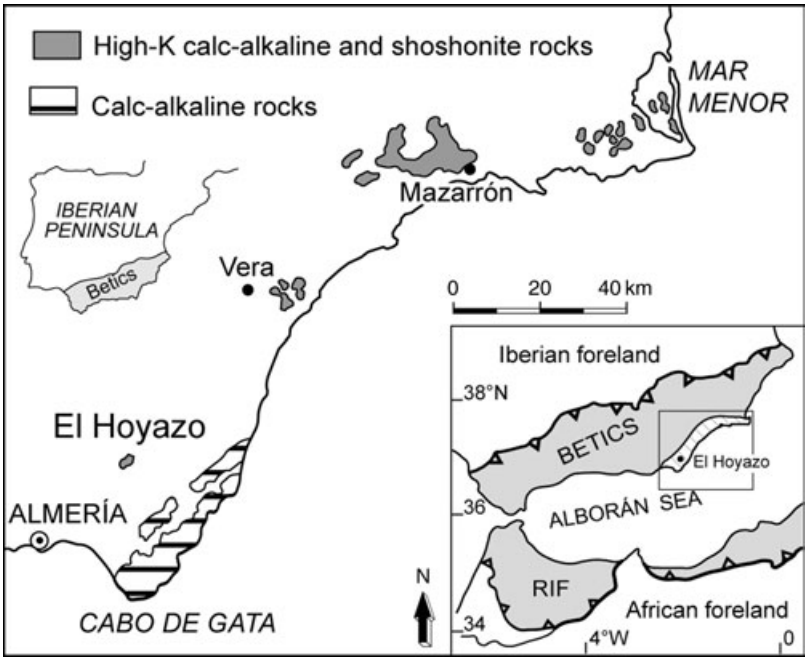

Fig. 1. Geographical location and schematic tectonic elements of the main edifices of the Miocene volcanics of the Neogene Volcanic Province within the Alborán Domain (after López-Ruiz & Rodríguez Badiola, 1980).

evolution which affected the Betic Cordillera during the Miocene. The Alborán Sea is an extensional basin where partial melting appears to have developed in a thinned continental crust after a major phase of lithospheric extension (Platt & Vissers, 1989; Vissers *et al*., 1995).

The NVP is mainly composed of calc-alkaline rocks, mostly andesites with minor high-K calc-alkaline to shoshonitic lava series (Fernández-Soler, 1996; Benito *et al*., 1999). Volcanism in the NVP ranges in age from 17 to 5 Ma (Zeck *et al*., 1998; Turner *et al*., 1999; Cesare *et al*., 2003a). The high-K calc-alkaline Grt–Crd (mineral abbreviations after Kretz, 1983; Fib, fine-grained acicular sillimanite, according to the definition of Pattison (1992); M = melt) bearing lavas, mostly dacites, crop out as scattered, small volcanic extrusions, aligned within a SW-NE trending zone that extends for *c*. 200 km at the south-eastern margin of Spain. In addition to El Hoyazo, high-K calc-alkaline lavas outcrop also at Vera, Mazarrón and Mar Menor, but elliptical garnet does not occur in the residual enclaves at these localities.

El Hoyazo is an extinct volcano with a volume of erupted volcanics of *c*. 1 km^3. The total content of foreign material (enclaves and xenocrysts) and mainly residual enclaves amount to *c*. 10–15 vol.% of the lava (Zeck, 1992). The high-K dacitic lava and most of its enclaves are interpreted to be co-genetic products from the partial melting of graphitic metapelites, as originally proposed by Zeck (1970). The magma has, however, been contaminated with mafic melt (Benito *et al*., 1999; López-Ruiz *et al*., 2002). The dacitic lavas typically contain centimetre-sized garnet, cordierite and quartz xenocrysts.

Crystalline fragments in El Hoyazo lava are medium to coarse-grained granulite facies rocks that range in size from a few tens of centimetres down to single xenocrysts. These are interpreted to be the result of fragmentation and dispersion in the host lava, possibly because of explosive emplacement. They have been characterized by Zeck (1968, 1970, who gave detailed petrographic descriptions and distinguished several types: Grt–Bt–Sil gneiss, Spl–Crd hornfels, Qtz–Crd rocks, schists–quartzites, and mafic inclusions. Graphite is also common. The first type is the most abundant and has been the subject of recent studies (Cesare *et al*., 2003a, and references therein). The Grt–Bt–Sil and Spl–Crd enclaves are strongly depleted in Si and enriched in Al and Fe (Zeck, 1968; Cesare *et al*., 1997; Benito *et al*., 1999) with respect to common metapelites such as those exposed in the adjacent Betic Cordillera. They have been interpreted as the residue after extraction of 35–60 wt% of rhyolitic glass from these metapelites (Cesare *et al*., 1997).

Available geothermometric determinations on the enclaves of El Hoyazo indicate equilibration at 850 ± 50 °C and 5.5–7 kbar (Cesare *et al*., 1997, 2003a), with a possible further heating event at >900 °C, testified by the microstructures of biotite melting to hercynitic spinel occasionally observed in some Grt–Bt–Sil enclaves (Cesare, 2000). SHRIMP ages obtained from zircon and monazite of the enclaves and their host dacite indicate that anatexis took place at *c*. 9.7 Ma, while the eruption has been dated at *c*. 6.3 Ma. Hence, the crustal glass resided for at least 3 Myr at an estimated depth of *c*. 25 km (Zeck & Williams, 2002; Cesare *et al*., 2003a).

One important aspect of the crustal enclaves of El Hoyazo is that they show evidence of having been intensely deformed during partial melting and melt extraction (Cesare *et al*., 1997; Cesare & Gómez-Pugnaire, 2001). In most cases, the foliation appears to be syn-anatectic. Most garnet occurs in these rocks as equidimensional, euhedral crystals. However, in a few Spl–Crd enclaves, garnet grains display elongated and elliptical shapes within layers with a pronounced foliation. In this paper we focus on these rocks.

PETROGRAPHY

The metapelitic Spl–Crd enclaves from El Hoyazo in which the elliptical garnet has been observed are fine to medium-grained rocks that show a well developed foliation, strongly folded in some cases (Cesare *et al*., 1997). The size of this type of residual fragment rarely exceeds 10 cm. These rocks are recognizable in the field because they form dark patches in the host lava. In hand specimen mainly sillimanite, small black spinel grains, cordierite porphyroblasts, biotite and garnet are observed.

Most garnet in the Spl–Crd samples is euhedral to subhedral and equidimensional. Elongate garnet is rare and only occurs in some samples with a well-developed foliation (Fig. 2a). The few samples with elongate (elliptical) garnet display strain and mineralogical

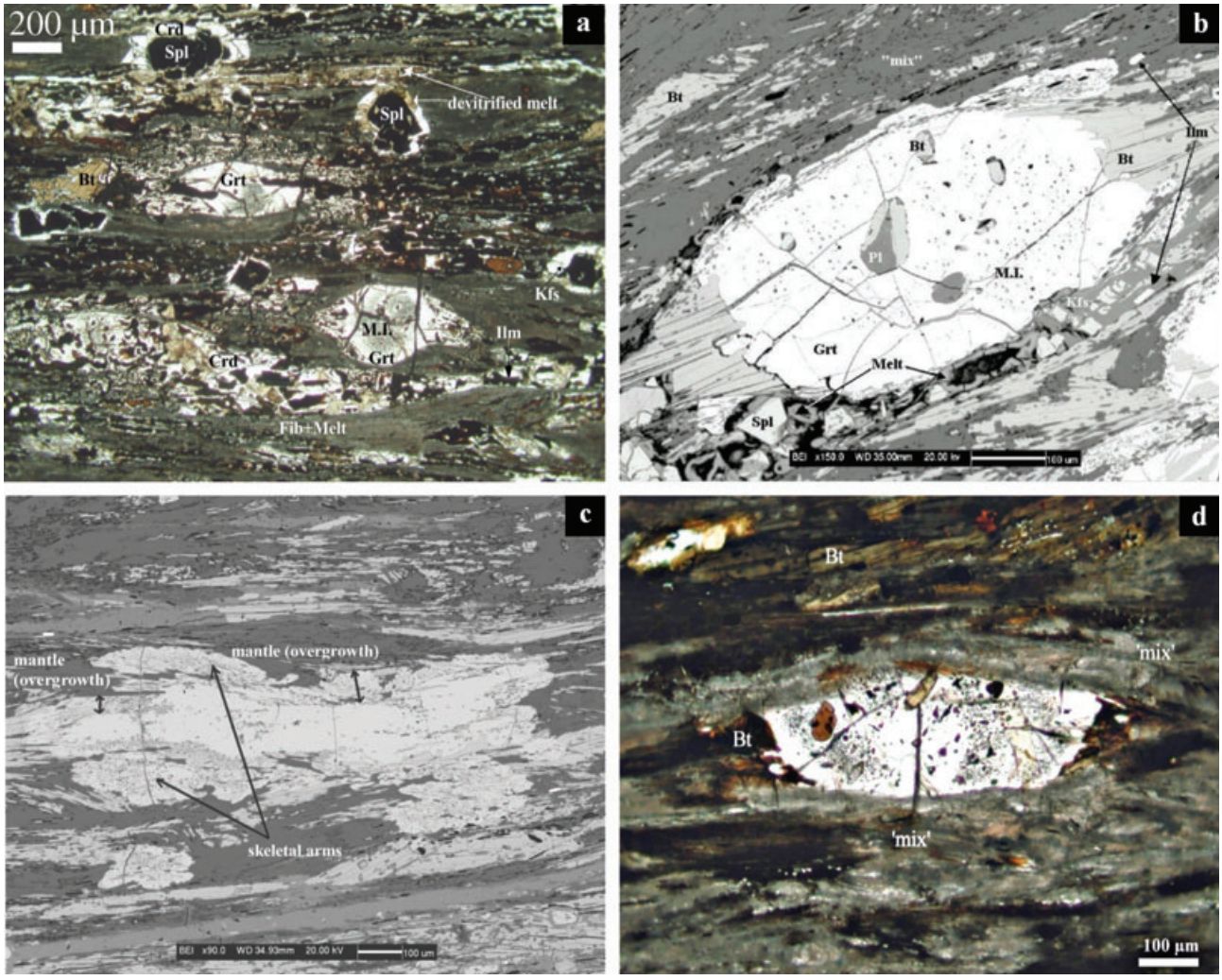

Fig. 2. (a) Microscopic general view of the studied rock, with evident porphyroblasts of garnet (Grt) and hercynitic spinel (Spl) in a foliated, E-W oriented matrix. The grey cores of garnet are areas rich of melt inclusions (MI). Plane-polarized light. (b) SEM-BSE view of an elliptical garnet. Strain shadows are composed of large oriented biotite crystals, while the strain caps are defined by layers of 'mix' (top) and/or devitrified glass (bottom). (c) SEM-BSE view of an elliptical garnet whose ratio is near to 4:1. Note that the overgrowth of the garnet mantle at the strain caps is less thick than the skeletal arms. (d) Photomicrograph of an elliptical garnet wrapped by a fibrolite-rich foliation matrix. In this optical image the garnet mantle cannot be resolved. The garnet is rich with inclusions of glass, biotite and graphite, which form a spherical shell, evidently truncated at the garnet strain caps. Plane-polarized light.

heterogeneities at the thin-section scale. The unfoliated zones contain euhedral garnet, cordierite, prismatic sillimanite and plagioclase. The elliptical garnet is elongated within the foliated layers (Fig. 2a,b), which also contain fibrolite, biotite and spinel. The garnet aspect ratios may reach up to 10:1. Figure 2c shows a BSE image of a typical elongate garnet with aspect ratio 4:1.

In this study, optical and SEM observations were critical in resolving some key textural relationships. Under the optical microscope, garnet forms single crystals, which appear to be wrapped by oriented layers of fibrolite, biotite, graphite and glass (Fig. 2a,d). SEM images, however, reveal that a garnet mantle overgrows fibrolite, biotite, graphite and glass (Fig. 3a). Corresponding SEM X-ray maps show a strong chemical zoning in the elongate garnet.

The *garnet core* is the inner part of the garnet. It is variable in size with high Mn content and low X_{Mg} [Mg/(Mg + Fe)], and typically contains primary inclusions of melt, biotite, ilmenite and graphite. The *garnet mantle* is the outer part of the garnet, poor in Mn and with higher X_{Mg} than the core. It frequently shows inclusions of fibrolite and graphite. Melt inclusions are not visible even in SEM-BSE images and Mn X-ray maps, and are absent in the garnet mantle. The garnet mantle overgrows the foliated matrix that wraps around the garnet core, including strain shadows and what appears to be former strain caps (Passchier & Trouw, 1996), rich in oriented matrix phase inclusions

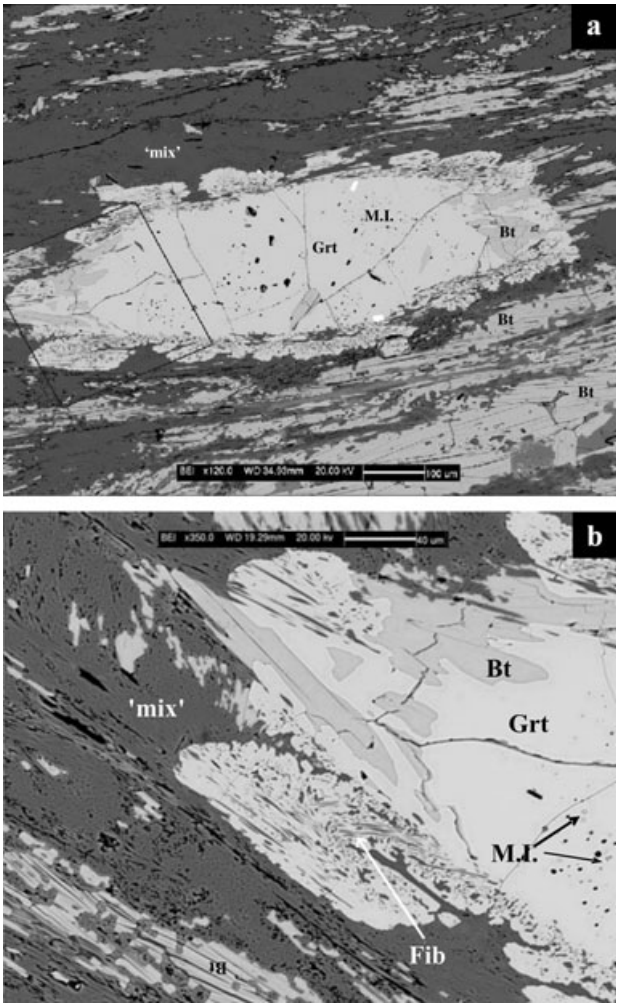

Fig. 3. (a) SEM-BSE image of a typical elliptical garnet. The elliptical core is surrounded by inclusion-rich overgrowths forming the mantle. Coarse-grained biotite is intergrown with garnet in the strain shadows. Rectangle corresponds to the enlargement of 'b'. (b) Close-up of the garnet mantle and strain shadow from 'a'. A skeletal arm includes a crenulated foliation outlined by fibrolite The foliation external to the garnet corresponds to the axial plane of the crenulation.

(e.g. Fig. 2b). In places, these garnet overgrowths form skeletal, elongated arms which extend along the foliation (Fig. 3).

Melt inclusions in the garnet core are very small, with maximum diameter of 10 μm, and are visible under both optical and BSE imaging (Figs 2a,b,d & 3). In the former case they occur as isotropic colourless inclusions, in the latter as darker areas within the bright garnet host. These inclusions are very similar to those reported and analysed in similar samples (Cesare *et al.*, 1997; Cesare & Gómez-Pugnaire, 2001; Cesare *et al.*, 2003c). In the present study, owing to their very fine grain-size, their identification as inclusions of glass has been made by qualitative EDS analysis under SEM. The melt inclusions generally have a dodecahedral shape, as reported from crystallized inclusions in garnet from granulites (e.g. Hartel *et al.*, 1990). Inclusions fulfil the textural criteria for primary trapping during growth of the host mineral, being arranged in shells within the garnet (Roedder, 1984). The occurrence of these melt inclusions shows that the garnet underwent crystallization in the presence of a glass phase during anatexis.

Primary melt inclusions in garnet cores commonly define a circular pattern that in some cases appears truncated at the interface with the biotite–fibrolite-rich strain caps (Fig. 2d). Locally, the circular pattern of melt inclusions forms a ring structure with melt inclusions being absent from the central part of the garnet core. The pattern of melt inclusions could mark the outer limit of the garnet core. However, it is apparent from Fig. 2d that the core extends asymmetrically outside the circular or random pattern of melt inclusions. This suggests either that a first phase of garnet growth produced a garnet core larger than the inclusion-rich zone, which was later dissolved asymmetrically by a strain-solution process, or that after the growth of the inclusion-rich zone, a process of strain-solution was accompanied by garnet reprecipitation in the strain-shadows. Typically the outer limit of the Mn-rich garnet core is defined by the occurrence of oriented biotite crystals, which constitute the strain shadows (see Figs 2b & 3b).

Where garnet occurs within biotite rich domains, the strain shadow of the elliptical microstructure is dominated by oriented biotite crystals (e.g. Fig. 2b). In summary, from a strain history point of view, the garnet core predates deformation and foliation development whereas the garnet mantle is either synchronous with or post-dates deformation. Cordierite encloses biotite, sillimanite, ilmenite, graphite and more rarely spinel. Cordierite also occurs around euhedral spinel crystals that overprint the foliation.

Biotite crystals occur both in the matrix and as inclusions in garnet (Fig. 2b). Regardless of its textural position, biotite shows strongly varying grain size, between a few microns and more than 100 μm. Biotite outside the garnet core is generally oriented parallel to the foliation. In the matrix it is oriented in bands or layers, more or less separated from Kfs + M + Spl + Fib, but sometimes also intergrown with the other phases, especially with fibrolite. Biotite commonly is related with thin K-feldspar layers along the cleavage planes

Fibrolite is the major matrix phase in view of its modal abundance, and is the mineral, which preferably defines the foliation. It generally forms a fine-grained, sponge-like aggregate where it is mixed with glass (Figs 2d & 3). This feature of these and other enclaves from the NVP has been defined as 'mix' by Cesare *et al.* (1997). Fibrolite is locally enclosed by cordierite, garnet and spinel and commonly outlines the elliptical shape of garnet (Fig. 2d). It also defines microfolds within the foliation overgrown by the garnet mantle

(Fig. 3b). Coarser prismatic sillimanite is rare and occurs as crystals which locally transect all other phases except for the latest biotite with which it is intergrown. It is common in unfoliated domains and appears to be texturally late.

The former glass phase in the matrix commonly occurs as devitrified glass, but locally forms fresh interstitial pockets with a rhyolitic composition. It also forms inclusions in most minerals. K-feldspar occurs in thin layers oriented within the foliation, and as thin layers that appear to have replaced biotite along cleavage planes. K-feldspar is also associated with spinel in textures overprinting the main foliation. Plagioclase is rare in these samples. It occurs within the matrix as elongate crystals parallel to the foliation, and also as small inclusions in biotite and garnet. Graphite is abundant; it typically occurs in continuous layers in the matrix following the foliation, and is enclosed by most solid phases. It locally also occurs within the garnet core. Euhedral spinel crystals display coronas of K-feldspar, cordierite or garnet, and overgrow the foliation. Anhedral crystals are smaller, do not form part of any corona and are intergrown with the matrix composed of fibrolite + biotite + glass, where they commonly form aggregates. Ilmenite crystals appear both enclosed by the garnet core and in the foliated matrix.

MINERAL CHEMISTRY

All phases, including glass, in the sample have been analysed using a Cameca Camebax electron microprobe (EMP) of Consiglio Nazionale delle Ricerche (CNR) at the Department of Mineralogy and Petrology of the University of Padova. Natural and synthetic silicates and oxides were used as standards, and data correction was performed using PAP methods as adapted by Cameca (Pouchon & Pichoir, 1984). Working conditions were 15 kV accelerating voltage and 15 nA sample current. The beam diameter was generally focused to *c.* 1 μm for solid phases, but was defocused to *c.* 5–10 μm for glass analysis.

Elliptical *garnet* is chemically zoned (Figs 4, 5 & Table 1), especially with respect to Mn content and X_{Mg}. This garnet displays a high Mn core with a rather constant composition ($Alm_{73-77}Prp_{7-11}Sps_{9-15}Grs_{2-4}$; $X_{Mg} = 0.09–0.13$). Mantle compositions have a lower Mn and a more restricted compositional range which is characterised by $Alm_{76-81}Prp_{11-14}Sps_{2-6}Grs_{3-5}$ and an $X_{Mg} = 0.13–0.15$. The Mn and X_{Mg} change from core to mantle is quite sharp (see Figs 5 & 6). By contrast, the grossular component is similar in core and mantle (0.03–0.06).

Biotite has high, but variable TiO_2 contents, ranging from 3.49 to 8.51 wt%, (0.21–0.52 atom PFU; Table 1) without a systematic relation to its microstructural location (i.e. related to garnet as strain shadows, strain caps and inclusions, and in the matrix). X_{Mg} of biotite ranges from 0.26 to 0.41. In the absence of a systematic pattern, these large variations probably reflect a chemical control from the local microdomain on biotite chemistry, and conditions of local equilibrium. F and Cl contents are low: < 0.48 wt% and below the detection limit, respectively. Biotite analyses show high totals ($> 97\%$), which can be explained by a hydrogen deficiency not correlated to an increase in halogens, such as documented in other samples by Cesare *et al.* (2003b). Cordierite crystals are unzoned and have X_{Mg} values of 0.43–0.47. Spinel is hercynite-rich solid solution with compositions in the range Hc_{78-80} $Spl_{13-19}Gah_{0-4}$. The range of X_{Mg} is 0.13–0.18.

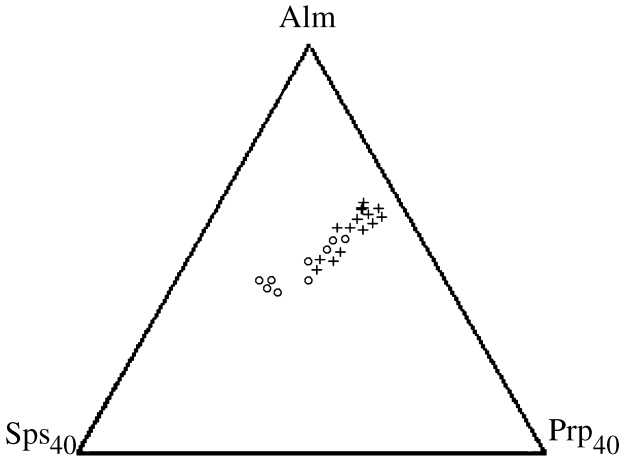

Fig. 4. Alm–Prp–Sps composition diagram with datapoints from the elliptical garnet (circles = Grt core; crosses = Grt mantle).

Plagioclase crystals show a compositional range from An_{37} to An_{65}. This large variation is not systematically correlated with the microstructural position of plagioclase. This could suggest, similarly to the case of biotite, that there is a chemical control from the local availability of Na and Ca in each microdomain. The K-content of plagioclase ranges from 3 to 8 mol of orthoclase component. K-feldspar crystals have composition in the range $Or_{84-87}Ab_{12-14}An_{<2}$.

The *glass* in both fresh interstitial pockets and within melt inclusions has a peraluminous rhyolitic composition. Table 1 only reports values from interstitial glass because melt inclusions within garnet generally give analyses of unacceptable quality as they are too small to be analysed with EMP. The oxide total suggests *c.* 3 wt% H_2O (see Table 1), and H_2O undersaturated conditions.

THERMOMETRIC CONSTRAINTS

Constraints on the *P–T* history of elliptical garnet can be derived from: ternary feldspar thermometry; intracrystalline cation distribution; and Fe–Mg exchange thermometry for Grt–Bt and Grt–Crd pairs. Using the solvus curves of Nekvasil & Burnham (1987) at the

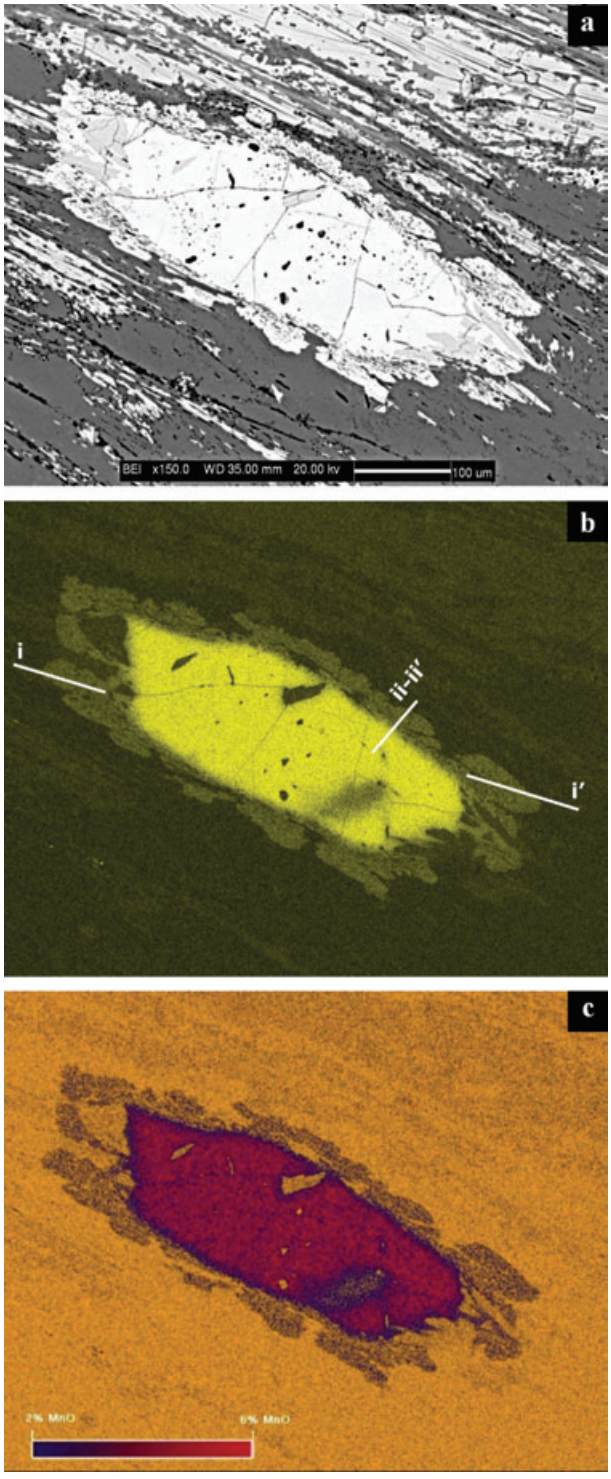

Fig. 5. Microstructures and chemical zoning pattern of the same elliptical garnet as in Fig. 2d. (a) SEM-BSE image. (b) SEM Mn X-ray map, with traces of chemical profiles *i–i′* and *ii–ii′* as reported in Fig. 6. (c) Quantitative MnO map elaborated from Fig. 5b. Note the homogeneous, high-Mn core (red) and strain shadows of garnet, a thin, low-Mn, inclusion-free inner rim (blue), and the low-Mn, inclusion-rich skeletal arms, which overgrow the matrix (orange) projecting preferentially parallel to the foliation.

arbitrary pressure of 5 kbar, the feldspar compositions indicate a range of minimum temperature of crystallization of 800–900 °C in the ternary feldspar diagram of Fig. 7. These values are almost pressure-independent.

A further way to evaluate temperature is by the estimate of Mg–Al–Fe distribution among T- and M-sites of spinel (Lavina *et al.*, 2003), by means of crystal structure and microchemical data. The cation distribution in natural spinel, compared with data from experiments in synthetic end members, gives an estimation of the closure temperature of the ordering reaction, i.e. a minimum temperature for the formation of spinel in the rock. Application of this technique to the hercynitic spinel from the elliptical garnet samples has provided $T > 800$ °C (B. Lavina, pers. comm.). The Grt–Crd thermometer of Nichols *et al.* (1992) provides a comparable temperature range, which may therefore be considered a reliable estimate of temperature in the enclaves.

In addition, Grt–Bt thermometery has been applied to touching mineral pairs located within the core, in intermediate portions and along the rim of elliptical garnet, with the purpose of checking for systematic temperature variations across grains. The temperatures obtained depend on the calibration used, which may provide values as low as 500 °C and as high as 1200 °C. The calibration of Ferry & Spear (1978) gives temperature values which mostly agree with the temperature range of 800–900 °C obtained from the other independent thermometers used, and thus it has been considered as the most reliable. It is worth mentioning that other calibrations (e.g. Indares & Martignole, 1985), which should account for the effect of Ti at high-T conditions, provided *c.* 200 °C lower temperatures. Using the reference calibrations of Ferry & Spear (1978) and Perchuk & Lavrent'eva (1983), results indicate that the garnet mantles have formed at slightly systematic higher temperature (up to 100 °C) than the garnet cores, implying that these two garnet generations probably developed in well-separated time periods. The high temperature values obtained above are consistent with the presence of melt throughout the evolution of elliptical garnet.

DISCUSSION AND INTERPRETATION OF RESULTS: A GENETIC MODEL

Elongated shapes in garnet have been mainly studied in medium-grade mylonites and in granulite facies rocks affected by high-strain conditions (Prior, 1993; Ji & Martignole, 1994; Kleinschrodt & Mcgrew, 2000). This paper presents another case, where garnet forms elongate shape under high-strain conditions coeval with anatexis.

As the elliptical garnet at El Hoyazo appear to have been affected by strain at high-T it is important to resolve whether or not they experienced any intracrystalline deformation. Electron backscatter

Table 1. Representative electron microprobe analyses of the analysed minerals.

	Grt c	Grt m	Grt c	Grt m	Grt c	Grt m	Bt	Bt	Crd	Crd	Kfs	Pl	Pl	Hc	Hc	Melt	Melt
SiO_2	36.88	37.19	37.37	37.41	37.36	37.34	33.92	33.83	48.01	47.63	64.77	53.98	55.01	0.00	0.02	76.15	75.13
TiO_2	0.07	0.10	0.04	0.06	0.00	0.14	5.94	6.57	0.00	0.07	0.00	0.01	0.02	0.28	0.16	0.13	0.18
Al_2O_3	20.69	21.14	20.86	21.22	21.75	22.28	18.65	18.50	32.17	32.26	18.87	28.81	27.21	57.06	56.77	12.34	12.04
Cr_2O_3	0.00	0.00	0.04	0.01	0.00	0.08	0.09	0.02	0.07	0.06	0.02	0.00	0.02	0.02	0.13	0.00	0.08
FeO	32.55	36.26	33.18	35.60	32.80	35.43	24.54	24.18	12.79	12.00	0.20	0.15	0.16	37.25	36.60	1.10	1.42
MnO	6.26	1.25	6.29	1.19	6.49	1.01	0.10	0.22	0.10	0.26	0.00	0.00	0.06	0.11	0.17	0.00	0.00
MgO	2.22	3.47	1.98	3.59	1.96	3.59	5.81	5.38	5.81	5.94	0.00	0.02	0.00	3.66	3.23	0.05	0.06
CaO	1.38	1.26	1.40	1.39	1.38	1.32	0.00	0.02	0.05	0.07	0.32	11.53	10.53	0.02	0.02	0.61	0.80
Na_2O	0.00	0.00	0.00	0.00	0.06	0.06	0.40	0.38	0.04	0.06	1.51	4.57	5.11	0.03	0.03	1.26	1.03
K_2O	0.03	0.04	0.00	0.03	0.00	0.09	8.78	8.97	0.14	0.24	13.86	0.70	0.91	0.06	0.00	4.95	4.33
ZnO														0.48	1.74		
Total	100.09	100.72	101.15	100.51	101.80	101.34	98.23	98.07	99.21	98.59	99.56	99.77	99.04	98.97	98.87	96.59	95.08
			24(O)				11(O)		18(O)			8(O)		4(O)			
Si	5.98	5.94	6.01	5.98	5.95	5.90	2.65	2.66	5.01	4.99	2.98	2.45	2.51	0.00	0.00		
Ti	0.01	0.01	0.00	0.01	0.00	0.02	0.35	0.39	0.00	0.01	0.00	0.00	0.00	0.01	0.00		
Al	3.95	3.98	3.95	4.00	4.08	4.15	1.72	1.72	3.95	3.98	1.02	1.54	1.46	1.94	1.94		
Cr	0.00	0.00	0.00	0.00	0.00	0.00	0.01	0.00	0.01	0.01	0.00	0.00	0.00	0.00	0.00		
Fe^{2+}	4.41	4.84	4.46	4.76	4.37	4.68	1.56	1.54	1.11	1.05	0.01	0.01	0.01	0.90	0.89		
Mn	0.86	0.17	0.86	0.16	0.88	0.14	0.01	0.00	0.01	0.02	0.00	0.00	0.00	0.00	0.00		
Mg	0.54	0.83	0.47	0.85	0.47	0.85	0.68	0.63	0.90	0.93	0.00	0.00	0.00	0.16	0.14		
Ca	0.24	0.22	0.24	0.24	0.24	0.22	0.00	0.00	0.01	0.01	0.02	0.56	0.52	0.00	0.00		
Na	0.00	0.00	0.00	0.00	0.01	0.01	0.06	0.06	0.01	0.01	0.13	0.40	0.45	0.00	0.00		
K	0.01	0.01	0.00	0.01	0.00	0.02	0.85	0.90	0.02	0.03	0.81	0.04	0.05	0.00	0.00		
Zn														0.01	0.04		
X_{Mg}	0.11	0.15	0.10	0.15	0.10	0.15	0.30	0.29	0.45	0.47				0.15	0.14		
Alm	0.73	0.80	0.74	0.79	0.73	0.80											
Sps	0.14	0.03	0.14	0.03	0.15	0.02											
Grs	0.04	0.04	0.04	0.04	0.04	0.04											
Prp	0.09	0.14	0.08	0.14	0.08	0.14											
X_{Ab}											0.14	0.40	0.44				
X_{An}											0.02	0.56	0.50				
X_{Or}											0.84	0.04	0.05				
ASI																1.81	1.95

Grt c = core; Grt m = mantle. Mineral formulae are based on the number of oxygen as given in the brackets. All iron as FeO.

diffraction (EBSD) analysis and orientation contrast (OC) images do not display any evidence of subdomains within the elliptical garnet. Therefore, we rule out the possibility of ductile deformation as a process responsible for the formation of the elongate garnet shapes, unless any former evidence of ductile deformation has been lost by high-T annealing during prolonged residence at depth.

Petrography, SEM-BSE images and Mn X-ray maps suggest a multistage evolution for elliptical garnet at El Hoyazo, from both chemical and textural points of view. Some of these garnet have a Mn-rich, elliptical core and a Mn-poor mantle overgrowing an anastomosing, Bt–Fib-rich foliation (Figs 3 & 5). During garnet growth, Mn is partitioned into garnet and thus becomes depleted in the matrix (Hollister, 1966). In our samples, Mn was strongly partitioned into garnet (Fig. 5) before strain, thus producing Mn-rich cores wrapped by the foliation. By the time the garnet overgrowths formed, there was little Mn left and they therefore have low Mn contents.

The elliptical garnet in the samples appear within pronounced foliation domains. However the primary melt inclusion patterns in the garnet core do not reflect any preferred orientation, but instead display a fairly circular pattern. This arrangement of inclusions suggests that garnet cores grew as idioblastic, equidimensional crystals, and that their growth was not mimicking a pre-existing foliation. Some garnet also shows truncation of the circular pattern of melt inclusions at strain caps on either side of the elliptical garnet cores. This truncation can be explained by high-T (melt-assisted) pressure solution at strain caps accompanied by (re)precipitation at strain shadows (Passchier & Trouw, 1996). Pressure-solution and truncation of the primary melt inclusion patterns may have been favoured by melt escape from garnet grain boundaries along the foliation planes (Cesare *et al.*, 1997).

The presence of a pronounced foliation is not necessarily evidence for tectonically induced strain. Volume loss also translates into strain (e.g. Ramsay, 1967), as is well known from compaction creep during diagenesis (Lehner, 1995) and in salt deformation experiments (Schutjens & Spiers, 1999). In migmatites and granulites, melt may escape from the partially molten system by mechanisms such as compaction and filter pressing (see review in Brown *et al.*, 1995), enhancing any pre-existing foliation. The loss of considerable amounts of glass (35–60%) in the enclaves of El Hoyazo is supported by mass-balance (Cesare *et al.*, 1997). The absence of melt inclusions in the garnet mantle can be explained also by this reason. The glass which formed part of the matrix, mixed with fibrolite needles, could escape by grain boundary flow before the static growth of the garnet mantle, while fibrolite

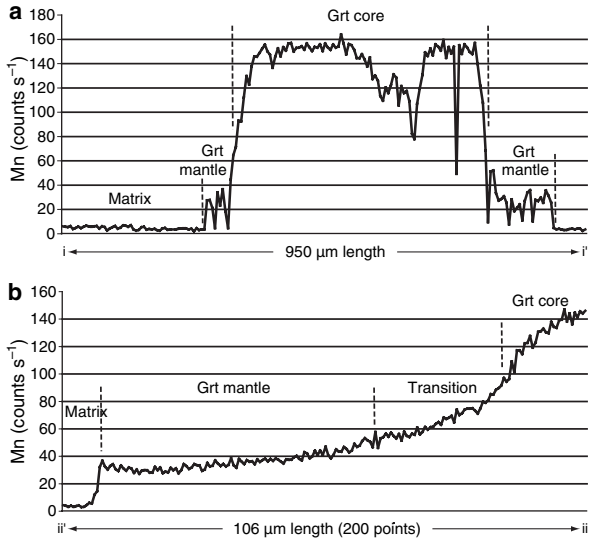

Fig. 6. Mn content (counts/sec) along profiles from Fig. 5b. Note: 164 count s^{-1} is *c.* 6.95 MnO wt%. (a) Profile *i–i′* includes from *i* toward *i′* the following parts: matrix, garnet mantle, garnet core, garnet mantle and matrix again. The core–mantle transition is represented by a sharp change in Mn content. (b) Detailed profile *ii–ii′*. It is focussed on the mantle–core transition in the garnet. Note that, the *ii–ii′* profile is not overlapping the *i–i′* one. The *ii–ii′* profile includes a small matrix part at the beginning followed by the garnet mantle and a part of the garnet core. The mantle–core transition is achieved within < 50 μm.

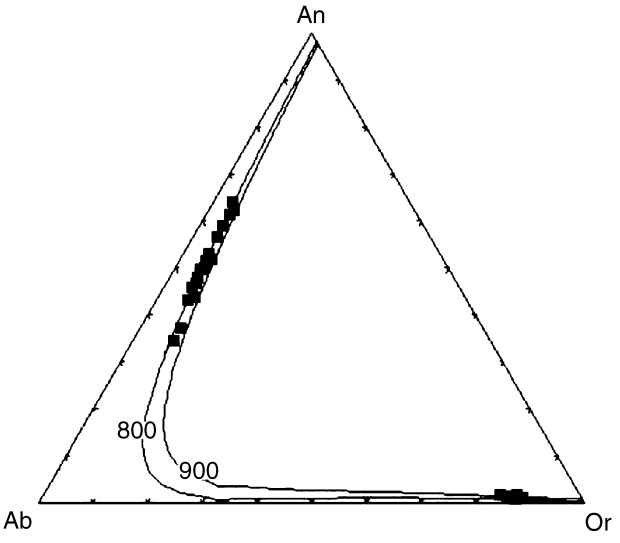

Fig. 7. Ab–An–Or diagram reporting the analysed feldspar compositions. Also plotted are the projections of the solvus at 800 and 900 °C, 5–7 kbar according to the model of Nekvasil & Burnham (1987).

crystals, oriented by this process of glass escape and 'inert' during garnet mantle growth were trapped as inclusions.

We propose a genetic model (Fig. 8) for the formation of elliptical garnet at El Hoyazo, consisting of a multistage evolution sequence at high-T (800–900 °C) in the presence of glass. In a first step, the high-Mn garnet cores grew equidimensionally trapping the anatectic glass as inclusions. A second step involved pressure-solution and (re)precipitation. Garnet was dissolved at strain cap, and was (re)deposited at strain shadows, thus producing the dominantly elongate shape of garnet cores, and the truncation of primary melt inclusion patterns in garnet. This process may have been promoted by melt escape from strain caps along foliation planes anastomosing around garnet cores (Fig. 2d). The third step is characterized by post-kinematic, partly mimetic overgrowth of low-Mn garnet forming the mantles, which typically enclose fibrolite, graphite and biotite from the matrix (Fig. 3).

Flat profiles of elements suggest chemical equilibration of minerals, which is commonly the result

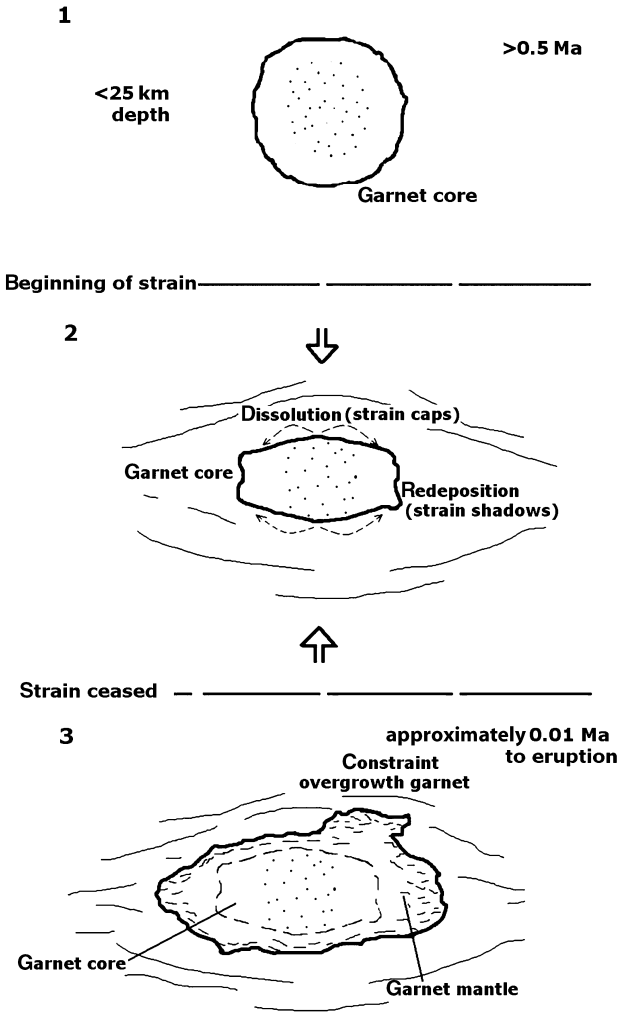

Fig. 8. Schematic time sequence of the elliptical garnet development. Step 1: Formation of an euhedral garnet core rich in Mn and primary melt inclusions. No strain conditions. Step 2: Dissolution of the garnet at strain caps and (re)precipitation at strain shadows during strain, causing an elliptical shape in the garnet. Step 3: Overgrowth of Mn-poor garnet after the strain is ceased.

of prolonged residence at high-T conditions (Chakraborty & Ganguly, 1991). As shown, the cores of elliptical garnet present flat, Mn-rich profiles (Fig. 6), whereas garnet mantles display flat, Mn-poor profiles (Fig. 6 & Table 1). However, the garnet core and mantle have not chemically homogenized with each other, their boundary being characterized by a sharp chemical change.

Homogenization of Mn profiles by diffusion in garnet cores that have radii <1 mm, should take *c*. 0.5 Myr at 850 °C, whereas it only takes 0.01 Myr to homogenize a <0.1 mm wide garnet mantle (e.g. Fig. 5) at the same temperature (Chakraborty & Ganguly, 1991). Hence, the samples may have remained at high temperature for *c*. 0.5–3.0 Myr after the core was produced, but must have cooled rapidly after the mantle had formed, so that there was not enough time to homogenise either the different formation temperature of cores and mantles, or the sharp change of Mn zoning. As rapid cooling of the enclaves is related to the eruption of the host dacite, it follows that the growth of garnet mantle occurred immediately (<0.01 Myr) before eruption. This can be matched with geochronological data on partial melting underneath, and eruption at El Hoyazo. Ion microprobe (SHRIMP) ages on monazite and zircon from the residual enclaves reveal a residence time of *c*. 3 Myr after partial melting at *c*. 25 km depth (Cesare *et al.*, 2003a).

In view of the Miocene geological evolution of the NVP, we do not rule out the possibility that the dacitic lava hosting the enclaves has changed the crustal levels of residence prior of its final eruption. In this case the garnet cores and mantles might have formed at, and might record different depths, so that the evolution of elliptical garnet is not isobaric.

The textural-chemical model together with the geochronological constraints not only help to extend the knowledge on garnet behaviour during crustal anatexis, but are also relevant for magma residence times at depth. This work also provides insights into the rheological response of anatectic rocks and into the possibility of formation of elliptical garnet by melt-assisted pressure-solution in granulites and migmatites.

ACKNOWLEDGEMENTS

Financial support from Universitá di Padova (Fondi Progetti Ricerca 2002) and CNR (Westmed Euromargins ESF Eurocore). Careful reviews by I. Braun, D. Pattison and M. Brown are gratefully acknowledged. We thank G. Pennacchioni for his critical pre-reading. We wish to acknowledge R. Spiess for introduction and help in the OC, EBSD techniques and other aspects related with this work; M.T. Gómez-Pugnaire, C. Ade, and B. Lavina for useful critical discussions; and R. Carampin for patient availability in the EMP.

REFERENCES

Benito, R., López-Ruiz, J., Cebriá, J.M. *et al.* 1999. Sr and O isotope constraints on source and crustal contamination in the high-K calc-alkaline and shoshonitic Neogene volcanic rocks of SE Spain. *Lithos*, **46,** 773–802.

Brown, M., Averkin, Y., Mclellan, E. & Sawyer, E., 1995. Melt segregation in migmatites. *Journal of Geophysical Research*, **100,** 15655–15679.

Cesare, B., 2000. Incongruent melting of biotite to spinel in a quartz-free restite at El Joyazo (SE Spain): textures and reaction characterization. *Contributions to Mineralogy and Petrology*, **139,** 273–284.

Cesare, B. & Gómez-Pugnaire, M. T., 2001. Crustal melting in the Alboran Domain: contraints from enclaves of the Neogene Volcanic Province. *Physics and Chemistry of the Earth A*, **26,** 255–260.

Cesare, B., Salvioli Mariani, E. & Venturelli, G., 1997. Crustal anatexis and melt estraction during deformation in the restitic enclaves at El Joyazo (SE Spain). *Mineralogical Magazine*, **67,** 15–27.

Cesare, B., Gómez-Pugnaire, M. T. & Rubatto D., 2003a. Residence time of S-type anatectic magmas beneath the Neogene Volcanic Province of SE Spain: a zircon and monazite SHRIMP study. *Contributions to Mineralogy and Petrology*, **146,** 28–43.

Cesare, B., Cruciani, G. & Russo U., 2003b. Hydrogen deficiency in Ti-rich biotite from anatectic metapelites (El Joyazo, SE Spain): crystal-chemical aspects and implications for high-temperature petrogenesis. *American Mineralogist*, **88,** 583–595.

Cesare, B., Marchesi, C., Hermann, J. & Gomez-Pugnaire, M. T., 2003c. Primary melt inclusions in andalusite from anatectic graphitic metapelites: implications for the position of the Al_2SiO_5 triple point. *Geology*, **31,** 573–576.

Chakraborty, S. & Ganguly, J., 1991. Compositional zoning and cation diffusion in aluminosilicate garnets. In: *Diffusion, Atomic Ordering and Mass Transport – Selected Problems in Geochemistry. Advances in Physical Geochemistry*. **8,** (ed. Ganguly, J.), pp. 120–170. Springer, Berlin, Germany.

Den Brok, S. W. J., 1998. Effect of microcracking on pressure solution strain rate: The Gratz grain-boundary model. *Geology*, **26,** 915–918.

Fernández-Soler, J. M., 1996. El volcanismo calco-alcalino en el parque natural de Cabo de Gata-Níjar (Almería). Estudio Volcanológico y Petrológico. *Sociedad Almeriense de Historia Natural. Monografías del Medio Natural*, **2,** 1–295.

Ferry, J. M. & Spear, F. S., 1978. Experimental calibration of the partitioning of Fe and Mg between biotite and garrnet. *Contributions to Mineralogy and Petrology*, **66,** 113–117.

Hartel, T. H. D., Pattison D. R. M., Helmers, H. & Maaskant, P., 1990. Primary granitoid-composition inclusions in garnet from granulite facies metapelite: Direct evidence for the presence of a melt? *Geological Association of Canada, Program with Abstracts*, **15,** A54.

Hollister, L. S., 1966. Garnet zoning: an interpretation based on the Rayleigh fractionation model. *Science*, **154,** 1647–1651.

Indares, A. & Martignole, J., 1985. Biotite–garnet geothermometry in the granulite facies: the influence of Ti and Al in biotite. *American Mineralogist*, **70,** 272–278.

Ji, S. & Martignole, J., 1994. Ductility of garnet as an indicator of extremely high temperature deformation. *Journal of Structural Geology*, **16,** 985–996.

Ji, S. & Martignole, J., 1996. Ductility of garnet as an indicator of extremely high temperature deformation: reply. *Journal of Structural Geology*, **18,** 1375–1379.

Kamb, W. B., 1959. Theory of preferred orientation developed by crystallization under stress. *Journal of Geology*, **67,** 153–170.

Kleinschrodt, R. & Mcgrew, A. J., 2000. Garnet plasticity in the lower continental crust: Implications for deformation mechanisms based on microstructures and SEM electron

channeling pattern analysis. *Journal of Structural Geology*, **22,** 795–809.
Kretz, R., 1983. Symbols for rock-forming minerals. *American Mineralogist*, **68,** 277–279.
Lavina, B., Koneva, A., & Della Giusta, A., 2003. Cation distribution and cooling rates of Cr-substitutes Mg–Al spinel from the Olkhon metamorphic complex, Russia. *European Journal of Mineralogy*, **15,** 435–441.
Lehner, F. K., 1995. A model for intergranular pressure solution in open systems. *Tectonophysics*, **245,** 153–170.
López-Ruiz, J., Cebriá, J. M. & Doblas M., 2002. Cenozoic volcanism I: the Iberian peninsula (Chapter 17). In: *The Geology of Spain*. (eds Gibbons, W. & Moreno, T.). Geological Society, London, UK.
Nekvasil, H. & Burnham, C. W., 1987. The calculated individual effects of pressure and water content on phase equilibiria in the granite system. In: *Magmatic Processes: Physicochemical Principles* (ed. Mysen, B.O.). Geochemical Society, University Park, PA, USA.
Nichols, G. T., Berry, R. F. & Green D. H., 1992. Internally consistent gahnitic spinel–cordierite–garnet equilibria in the FMASH Zn system: geothermobarometry and applications. *Contributions to Mineralogy and Petrology*, **111,** 362–367.
Passchier, C. W. & Trouw, R. A. J., 1996. *Microtectonics*. Springer-Verlag, Heidelberg.
Pattison, D. R. M., 1992. Stability of andalusite and sillimanite and the Al2SiO5 triple point: Constraints from the Ballachulish aureole, Scotland. *Journal of Geology*, **100,** 423–446.
Perchuk, L. L., & Lavrent'eva, I. V., 1983. Experimental investigation of exchange equilibria in the system cordierite–garnet–biotite. In: *Kinetics and Equilibrium in Mineral Reactions* (ed Saxena, S.K.), pp. 199–240. APG Series, Springer.
Platt, J. P. & Vissers, R. L. M., 1989. Extensional collapse of thickened continental lithosphere: a working hypothesis for the Alborán Sea and Gibraltar arc. *Geology*, **17,** 540–543.
Pouchon, J. L. & Pichoir, F., 1984. Un nouveau modéle de calcul pour la microanalise quantitative par spectrométrie de rayon-X: I. Application á l'analyse d'échantillons homogènes. *La Recherche Aérospatiale*, **3,** 167–192.
Prior, D. J., 1993. Sub-critical fracture and associated retrogression of garnet during mylonitic deformation. *Contributions to Mineralogy and Petrology*, **113,** 545–556.
Prior, D. J., Boyle, A. P., Brenker, F. *et al.* 1999. The application of electron backscatter diffraction and orientation contrast imaging in the SEM to textural problems in rocks. *American Mineralogist*, **84,** 1741–1759.
Ramsay, J. G., 1967. *Folding and Fracturing of Rocks*. McGraw-Hill.
Roedder, E., 1984. *Fluid Inclusions. (Reviews in Mineralogy, 12)*. Mineral Society of America, Washington, DC, USA.
Schutjens, P. M. T. M. & Spiers, C. J., 1999. Intergranular pressure-solution in NaCl: Grain-to-grain contact experiments under the optical microscope. *Oil & Gas Science Technology*, **45,** 729–750.
Sprunt E. S. & Nur A., 1977. Experimental study of the effects of stress on solution rate. *Journal of Geophysical Research*, **82,** 3013–3022.
Tada, R. & Siever, R., 1989. Pressure solution during diagenesis. *Annual Reviews of Earth and Planetary Science*, **17,** 89–118.
Turner, S. P., Platt, J. P., George, R. M. M., Kelley, S. P., Pearson, D. G. & Nowell G. M., 1999. Magmatism associated with orogenic collapse of the Betic-Alborán Domain, SE Spain. *Journal of Petrology*, **40,** 1011–1036.
Twiss, R. J. & Moores, E. M., 1992. *Structural Geology*. W. H. Freeman and Company.
Vissers, R. L. M., Platt, J. P. & Van Der Wal, D., 1995. Late orogenic and compositional constraints on 'post orogenic' magmatism. Geology extension of the Betic Cordillera and the Alborán Domain: a lithospheric view. *Tectonics*, **14,** 786–803.
Zeck, H. P., 1968. *Anatectic Origin and Further Petrogenesis of Almandine-bearing Biotite Cordierite–Labradorite–Dacite with Many Inclusions of Restite and Basaltoid Material, Cerro de Hoyazo, SE Spain*. PhD Thesis, Amsterdam, the Netherlands.
Zeck, H. P., 1970. An erupted migmatite from Cerro de Hoyazo, SE Spain. *Contributions to Mineralogy and Petrology*, **26,** 225–246.
Zeck, H. P. 1992. Restite-melt and mafic-felsic magma mingling in an S-type dacite, Cerro del Hoyazo, southeastern Spain. *Transactions of the Royal Society of Edinburgh, Earth Science*, **83,** 139–144.
Zeck, H. P. & Williams, I. S., 2002. Inherited and magmatic zircon from Neogene Hoyazo cordierite dacite, SE Spain – Anatectic source rock provenance and magmatic evolution. *Journal of Petrology*, **43,** 1089–1104.
Zeck, H. P., Kristensen, A. B. & Williams, I. S., 1998. Post-collisional volcanism in a sinking slab setting – crustal anatectic origin of pyroxene–andesite magma, Caldear Volcanic Group, Neogene Alborán volcanic Province, southeastern Spain. *Lithos*, **45,** 499–522.

Received 20 May 2004; revision accepted 30 November 2004.